Title: An optimized geometry for a micro Penning-trap mass spectrometer based on interconnected ions

Author: J.M. Cornejo M.J. Gutiérrez E. Ruiz A. Bautista-Salvador C. Ospelkaus S Stahl D. Rodríguez

PII: S1387-3806(16)30217-2
DOI: http://dx.doi.org/doi:10.1016/j.ijms.2016.10.010
Reference: MASPEC 15689

To appear in: *International Journal of Mass Spectrometry*

Received date: 6-7-2016
Revised date: 6-10-2016
Accepted date: 11-10-2016

Please cite this article as: J.M. Cornejo, M.J. Gutiérrez, E. Ruiz, A. Bautista-Salvador, C. Ospelkaus, S Stahl, D. Rodríguez, An optimized geometry for a micro Penning-trap mass spectrometer based on interconnected ions, *<![CDATA[International Journal of Mass Spectrometry]]>* (2016), http://dx.doi.org/10.1016/j.ijms.2016.10.010

An optimized geometry for a micro Penning-trap mass spectrometer based on interconnected ions

J.M. Cornejo[a,1], M.J. Gutiérrez[a], E. Ruiz[a,2], A. Bautista-Salvador[b,c], C. Ospelkaus[b,c], S Stahl[d], D. Rodríguez[a,e,*]

[a] *Departamento de Física Atómica, Molecular y Nuclear, Universidad de Granada, 18071, Granada, Spain*
[b] *Physikalisch-Technische Bundesanstalt, Bundesallee 100, 38116, Braunschweig, Germany*
[c] *Institute of Quantum Optics, Leibniz Universität Hannover, Welfengarten 1, 30167 Hannover, Germany*
[d] *Stahl-Electronics, 67582 Mettenheim, Germany*
[e] *Centro de Investigación en Tecnologías de la Información y las Comunicaciones, Universidad de Granada, 18071, Granada, Spain*

Abstract

The Penning-trap mass spectrometers providing the highest sensitivity are based on electronic detection and amplification of the electric current a stored ion induces in the trap electrodes. This technique allows for very precise mass measurements using a single ion in the trap, but it has not been yet demonstrated with a singly-charged heavy ion. The work presented in this paper is aiming at building a novel Penning-trap system, where the electronic detection is substituted by the detection of fluorescence photons from a laser-cooled $^{40}Ca^{+}$ (sensor) ion. This will allow extending the applicability of single-ion Penning trap mass spectrometry to any ion, regardless its mass or charge, which is a pre-requisite to perform precise mass measurements on heavy and super-heavy elements. The system, developed in the framework of the project TRAPSENSOR at the University of Granada, is comprised of two traps, one to store the probed ion and the other to store the sensor one. This paper reports on theoretical studies carried out to optimize the geometry of this double micro Penning-trap system, which has been built together with the electronics.

Keywords: Ion traps, Laser cooling, Penning-trap mass spectrometry, Induced image current, Ion-ion coupling

1. Introduction

Highly accurate mass measurements on atomic and molecular ions by means of Penning traps have been utilized, in combination with other measurements, for the determination of fundamental constants, to perform precision tests of Physics laws, and to measure fundamental properties of elementary particles [1, 2, 3, 4]. In all these Penning-trap experiments a single ion is detected non-destructively, using variants of the induced image-current (IIC) technique (see e.g. [5, 6, 7]). However, the IIC technique has been applied so far to ions with low or medium mass-to-charge ratios, and not to heavy or superheavy elements with 1^{+} electronic-charge state.

The lowest relative mass uncertainty reported with the IIC technique has been reached using $^{16}O^{6+}$ ($\delta m/m = 1.1 \times 10^{-11}$) [8]. The spectrometer is currently in operation at the Max Planck Institute for Nuclear Physics in Heidelberg aiming at measuring the masses of T^{+} and $^{3}He^{+}$ [9] to contribute to the determination of the mass of the electron antineutrino with a sensitivity of 0.2 eV/c^2, once these masses are combined with the decay measurements carried out by the international collaboration KATRIN (KArlsruhe TRItium Neutrino experiment) [10]. Extending the applicability of single-ion Penning trap mass spectrometry to singly-charged heavy ions is also of interest for similar experiments performed on the ion species involved in the decays from ^{187}Re to ^{187}Os [11] and from ^{163}Ho to ^{163}Dy [12, 13, 14], and it is highly desirable to perform mass measurements on Superheavy elements (SHE) produced in fusion-evaporation reactions with very low cross sections, since they are thermalized in a gas-filled stopping chamber and reach the measurement trap with an electronic-charge state of 1^{+} or 2^{+} [15, 16, 17]. The relative mass uncertainty for $^{187}Re^{+}$-$^{187}Os^{+}$ and $^{163}Ho^{+}$-$^{163}Dy^{+}$ has to be in the order of 10^{-12} to contribute to the determination of the neutrino mass, and just at the level of 10^{-7} for SHE studies.

A new method referred to as *Quantum Sensor* (QS), was proposed and described in detail in Ref. [18], in order to overcome the present mass limit in reach with the single-ion IIC technique. This method consists in replacing the resonant-circuit or SQUID, operated at 4 K, by a laser-cooled $^{40}Ca^{+}$ ion oscillating in a contiguous trap, with a motional energy of about 1 mK. The detection is done by monitoring the axial oscillation frequency through the fluorescence photons emitted by the laser-cooled $^{40}Ca^{+}$ ion, following the same principle as the method previously proposed by D.J. Heinzen and D.J. Wineland [19]. The radial degrees of freedom can be coupled to the axial one using side-band drives [6]. The interaction between the heavy or superheavy ion and $^{40}Ca^{+}$ oc-

*Corresponding author
Email address: danielrodriguez@ugr.es (D. Rodríguez)
[1] Present address: Institute of Quantum Optics, Leibniz Universität Hannover, Welfengarten 1, 30167 Hannover, Germany
[2] Present address: Departamento de Electrónica y Tecnología de Computadores, Universidad de Granada, 18071, Granada, Spain

curs through interconnected image-current sensing electrodes[3], and the ultra-low temperature of the $^{40}Ca^{+}$ ion will allow determining the ion motional frequencies from minute currents induced by an ion oscillating with very low amplitude in the potential well of the trap. The QS method can be applied to any mass-to-charge ratio, i.e., it is not limited by the resonance frequency of the detection circuit.

In order to provide efficient ion-ion coupling, the size of the trap, characterized by a parameter termed d has to be reduced with respect to the size of existing Penning-trap mass spectrometers (e.g. Ref. [8] where $d = 2.11$ mm). Regarding accuracy, the ratio between the oscillation amplitude of the ion and d must be kept small. The reduction of d is limited because of the shift of eigenfrequencies due to image charges, scaling this shift inversely as the inverse cube of the trap size, and linearly with the electronic-charge state of the ion [21, 22]. The stability of the magnetic field is also important, and this can be monitored in the whole volume of the two traps from the fluorescence signal emitted by the laser-cooled $^{40}Ca^{+}$ ion on probing one of its eigenfrequencies. This is possible due to the small size of the traps ($d = 1$ mm) and the large volume (1 cm^3) where the magnetic field is homogeneous to the 0.1 ppm level. The full system might be also built with a third trap so that the probed ion can be shuttled from/to the double microtrap system [23]. The layout of the facility to implement the QS at the University of Granada in the framework of the project TRAPSENSOR was shown in Ref. [24].

This paper will be devoted to study the suitability of a specific geometry to build the double micro Penning-trap mass spectrometer to improve sensitivity and to extend the applicability of single-ion Penning trap mass spectrometry. The geometry decided for the experiment has been also adapted to fit the microfabrication and assembly to electronics.

2. Electrostatic potential in a Penning trap

The Penning trap is a device where ions are confined by the combination of an electrostatic and a magnetic field [25]. A sketch of a possible implementation of the Penning trap is shown in the left side of Fig. 1. The trap in this figure is made of a central ring electrode and two endcaps shaped in a way to create an electrostatic quadrupole potential. The magnetic field $\vec{B}$ is in the axial direction ($\vec{z}$), and the voltages to generate the electrostatic potential are applied to the endcaps with respect to the ring electrodes. The right side in Fig. 1 illustrates the equipotential lines of the quadrupole field, which in the case of the hyperbolic Penning trap (left side of Fig. 1) follows the shape of the electrodes.

The motion of an ion with mass m and charge q in a Penning trap can be described as the superposition of three independent motions [25]. The oscillation amplitudes associated with these

[3]For laser cooling in an ion trap, see e.g. Ref. [20].

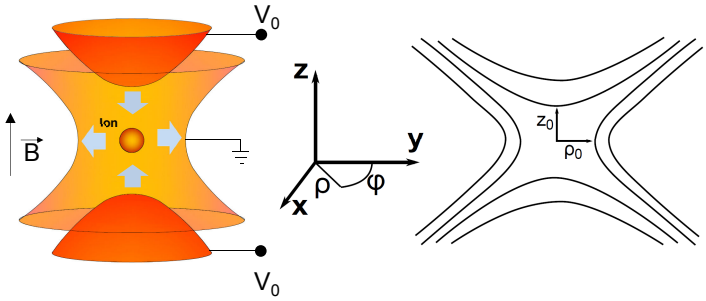

Figure 1: Left: Sketch of a hyperbolic Penning trap with revolution symmetry along the z axis. The thick arrows represent the direction of the forces the ion experiences due to the electrostatic field, which confines an ion in the axial direction (z). The magnetic field ($\vec{B}$) counteracts the effect of the electrostatic field in the radial direction (ρ). Right: Equipotential lines of the quadrupole field. z_0 and ρ_0 are the characteristic dimensions of the trap, which in the case of the hyperbolic Penning trap are defined as the distance from the electrode to the trap center.

motions are represented by ρ_+ (reduced-cyclotron), ρ_z (axial) and ρ_- (magnetron). The motion in the axial direction, parallel to the magnetic field lines, has the characteristic frequency

$$\nu_z = \frac{1}{2\pi}\sqrt{\frac{q\,V_0}{m\,d^2}}, \tag{1}$$

where V_0 is the potential difference between the endcap and the ring electrode, and d is defined as

$$d = \sqrt{\frac{1}{2}\left(z_0^2 + \frac{1}{2}\rho_0^2\right)}. \tag{2}$$

z_0 and ρ_0 are the characteristic dimensions of the trap shown in Fig. 1. The other two motional degrees of freedom are in the radial plane, and they are referred to as reduced-cyclotron, and magnetron motion with characteristic frequencies given by

$$\nu_+ = \frac{\nu_c}{2} + \sqrt{\frac{\nu_c^2 - 2\nu_z^2}{4}}, \tag{3}$$

and

$$\nu_- = \frac{\nu_c}{2} - \sqrt{\frac{\nu_c^2 - 2\nu_z^2}{4}}, \tag{4}$$

respectively. ν_c is the cyclotron frequency of an ion in a magnetic field in the absence of any electrostatic field, and is given by

$$\nu_c = \frac{1}{2\pi}\frac{q}{m}B, \tag{5}$$

which relates directly the mass-to-charge ratio of the ion to the observable frequency. In order to perform precise mass measurements, the magnetic field must be strong (on the order of several Tesla) and with an inhomogeneity on a ppm level in the center of the trap across the volume of the ion's motion. The frequency ν_c can be unfolded from the relationship

$$\nu_c^2 = \nu_z^2 + \nu_+^2 + \nu_-^2, \tag{6}$$

known as invariance theorem [25], which holds in any (non-ideal) Penning trap. The characteristic frequencies also follow

the relationship

$$\nu_+ \gg \nu_z \gg \nu_-. \tag{7}$$

A real Penning trap will have, in general, a different geometry than the one sketched in Fig. 1, and thus it is not straightforward to define V_0, z_0 and ρ_0. In order to obtain these parameters, the electrostatic potential can be expanded around the trap center, where the first and mixed-second order derivatives vanish due to the quadrupole symmetry. For the axial direction one can write:

$$V(z) \approx \frac{1}{2}\frac{\partial^2 V}{\partial z^2} z^2 = C_2\, z^2, \tag{8}$$

and

$$\nu_z = \frac{1}{2\pi}\sqrt{\frac{2\,q}{m} C_2}, \tag{9}$$

which can be used for any kind of trap instead of Eq. (1), regardless of the geometry. The coefficient C_2 will define the axial oscillation frequency which needs to be measured and also to be used to determine the other motional frequencies ν_+ and ν_- and in this way the mass of the probed ion.

Within the work presented in this manuscript, $V(x, y, z)$ has been obtained by solving Laplace's equation. Depending on the geometry of the trap, this equation can be solved analytically, directly or using Green's functions, or numerically.

3. Ion-ion interaction in the *Quantum-Sensor* approach

The *Quantum-Sensor* (QS) approach is schematically shown in Fig. 2 [18]. Since the detection procedure relies on the charges the ions induce in an interconnected image-current sensing electrode, one needs to consider the force which stems from the charge induced by the probed ion and the effect of this force on the sensor ion.

3.1. Force due to the probed ion

The potential ΔU due to the induced charge Q_{ind} by the probed ion in the interconnected image-current sensing electrodes will induce motion on the sensor ion, transferring energy and causing it to oscillate. This electric potential reads

$$\Delta U = \frac{Q_{ind}}{C_T}, \tag{10}$$

where C_T is the capacitance of the interconnected image-current sensing electrodes seen by the probed and sensor ions. Q_{ind} cannot be calculated directly, and it is necessary to integrate its time derivative. In the axial direction (z-axis and unit vector $\hat{e}_z$), the current induced for an ion with electronic charge q is given by

$$\dot{Q}_{ind} = \frac{\vec{v}_z \cdot q\vec{E}}{V'}, \tag{11}$$

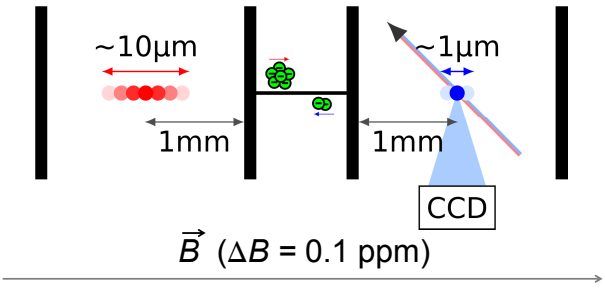

Figure 2: Schematics of the double micro Penning-trap mass spectrometer based on interconnected ions. Each trap is represented by two parallel plates perpendicular to the magnetic field axis. The homogeneity of the magnetic field is 0.1 ppm in a volume of 1 cm^3. The probed ion is depicted in red and the sensor one in blue. All the eigenfrequencies will be detected through the axial motion [18].

where $\vec{E}$ is the electric field due to the potential V' applied between the interconnected image-current sensing electrodes and the opposite ones, and $\vec{v}_z$, is the axial velocity of the ion in the trap which can be written as

$$\vec{v}_z = -\omega_z\, \rho_z \sin(\omega_z\, t)\, \hat{e}_z, \tag{12}$$

or equivalently like

$$\vec{v}_z = -\omega_z \sqrt{\frac{2qU_z}{m\omega_z^2}} \sin(\omega_z\, t)\, \hat{e}_z, \tag{13}$$

where qU_z is the axial energy of the ion. The ratio E/V' in Eq. (11), equals the inverse of the distance between the electrodes considering them as parallel plates. For a more general geometry, V' arises from the normalization of the electric field with respect to an unknown potential value. This is a result after unfolding the potential using Green's functions for a constant electrode. The expression for such a potential is

$$V(\vec{r}) = V'\, f(\vec{r}), \tag{14}$$

where $f(\vec{r})$ is a function which can be related to the electric field and the potential through

$$\frac{\vec{E}}{V'} = \frac{\partial f(\vec{r})}{\partial z}\hat{e}_z, \tag{15}$$

for a normalized field along the trapping axis. Q_{ind} can be calculated integrating Eq. (11). Using the result in Eq. (10), yields

$$\Delta U = \frac{\rho_z\, qE}{C_T\, V'} cos(\omega_z t). \tag{16}$$

3.2. Effect on the sensor ion

The potential induced in the interconnected image-current sensing electrodes is a harmonic function, and thus the energy transferred to the laser-cooled ion, provided this and the other ion

move with the same oscillation frequency, can be modeled as a forced oscillator, i.e., following the well-known equation

$$\frac{d^2z}{dt^2} + \omega_z^2 z = \frac{F_0}{m}\sin(\omega_z\, t)\,, \tag{17}$$

which has the general solution

$$z(t) = b\, t\cos(\omega_z\, t + \phi)\,, \tag{18}$$

where b represents the increase rate of the amplitude with time. This parameter is used to compare the strength of the ion-ion coupling among different geometries, since physically, the maximum amplitude is limited by the oscillation amplitude of the hotter ion. Inserting this equation into Eq (17), yields

$$b = \frac{F_0}{m}\frac{1}{2\,\omega}. \tag{19}$$

For any trap, F_0 can be written as the product of the charge and the field created by the potential ΔU. Combining the last equation with Eq. (15) and taking $V' = \Delta U$, one can obtain

$$b = \frac{q\,\Delta U}{m}\frac{1}{2\,\omega}\frac{\partial f(\vec{r})}{\partial z} \tag{20}$$

4. Micro-trap geometry

Different geometries for the double micro Penning-trap system have been studied (see Figs. 3 and 4). In all cases the axial frequency, ν_z was fixed at 100 kHz in order to have the parameter b, directly related to the time needed to exchange the energies between the sensor ion (cooled) and the probed ion (hot), as large as possible, within the limits imposed by the potentials applied to the electrodes (see Eq. (1)) [18]. Smaller trap size allows also for smaller times [19]. Besides the electrostatic quadrupole potential, the frequency and frequency stability, several issues are important to decide which geometry is the most suitable for the project TRAPSENSOR:

- Revolution symmetry around the magnetic field axis
- Optical access to the sensor ion in the radial direction
- Injection and capture of ions created outside the Penning-trap system
- Easy tuning for any mass-to-charge ratio
- Strong ion-ion coupling through the interconnected image-current sensing electrodes
- Small ρ_z-to-z_0 ratio

In the following, only the geometry referred to as open-ring trap will be presented. The outcomes from the other geometries studied (shown in Fig. 3) are summarized in Tab. 1.

The open-ring trap is an adapted version of the transparent Paul trap used in the project TRAPSENSOR to study Doppler cooling of the $^{40}Ca^+$ ion [26]. A technical drawing of the

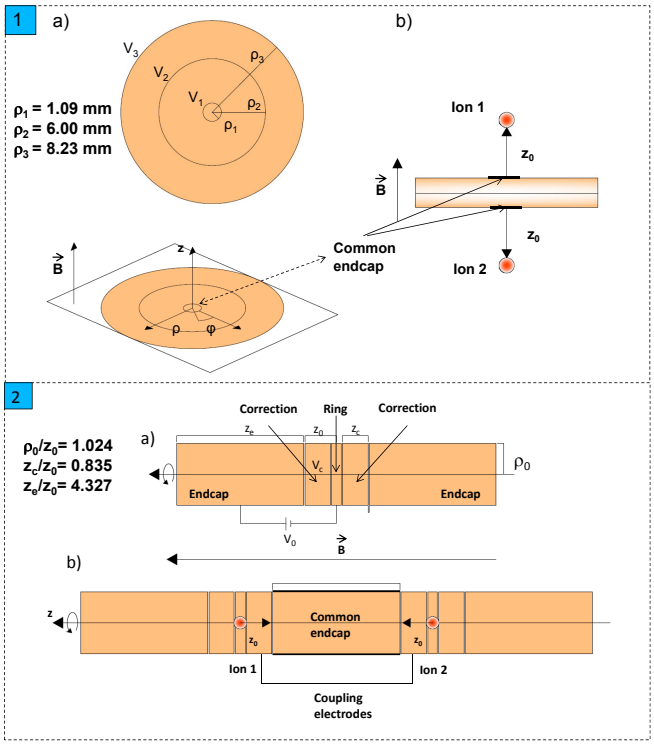

Figure 3: CAD drawings of standard trap geometries studied in this work for the development of the double micro Penning-trap spectrometer; a) configuration for a single trapped charged particle and b) projection for two ions stored in different traps. 1) Planar trap [27, 28] and 2) cylindrical trap [29].

longitudinal cut of the modified trap is shown in Fig. 4. The electrode added to the initial configuration is marked in red, and the new parameter L, is taken as a variable.

The potential function for this trap has no analytical solution and thus, the finite-difference method will be used (see e.g. [30]). The coefficients to calculate the frequency and its shift are obtained from a fit to the potential near the center of the trap ($\Delta z = \pm 4$ mm and $\Delta\rho = \pm 5$ mm), using a sixth order polynomial

$$\begin{aligned} V(\rho,\, z) = C_0 + C_2\left(z^2 - \frac{\rho^2}{2}\right) \\ + C_4\left(z^4 - 3\,\rho^2 z^2 + \frac{3}{8}\rho^4\right) \\ + C_6\left(z^6 - \frac{15}{2}\rho^2 z^4 + \frac{45}{8}\rho^4 z^2 - \frac{5}{16}\rho^6\right). \end{aligned} \tag{21}$$

The odd coefficients will vanish due to the symmetry around the z-axis. The coefficient C_4 is used to calculate the frequency shift

$$\Delta\nu_z = \frac{3\,q\,C_4\,k_B\,T}{16\,\pi^4\,m^2\nu_z^3}, \tag{22}$$

obtained in a similar way as using Eq. (9) for a non-hyperbolic trap [31]. The effects of higher order coefficients are negligible.

Table 1: Potential due to the charge induced in the interconnected image-current sensing electrodes (ΔU) and transfer constant (b) for the system $^{187}Re^{+}$-$^{40}Ca^{+}$ for different trap geometries. Two of the electrodes have been considered, for each to the trap geometries shown in Figs. 3 and 4. The energy of 0.025 eV corresponds to a temperature of 300 K. ΔU is calculated considering a $^{187}Re^{+}$ ion, while $^{40}Ca^{+}$ is used for the calculation of b. ρ_0 = 1 mm for cylindrical trap 1 and 1.5 mm for cylindrical trap 2.

	Planar Trap	Cylindrical Trap 1	Cylindrical Trap 2	Ring Trap
E (eV)	0.025	0.025	0.025	0.025
ΔU_1 (V)	1.69×10^{-9}	1.92×10^{-9}	1.10×10^{-9}	2.88×10^{-10}
b_1 ($\frac{m}{s}$)	1.32×10^{-6}	1.70×10^{-6}	5.55×10^{-7}	3.81×10^{-8}
Electrode 1	V_1 in Fig. 3	Correction in Fig. 3	Correction in Fig. 3	Coupling in Fig. 4
ΔU_2 (V)	9.38×10^{-10}	-	-	1.17×10^{-9}
b_2 ($\frac{m}{s}$)	4.04×10^{-7}	-	-	6.32×10^{-7}
Electrode 2	V_2 in Fig. 3	-	-	V_1 in Fig. 4
b_{total} ($\frac{m}{s}$)	1.72×10^{-6}	1.70×10^{-6}	5.55×10^{-7}	6.68×10^{-7}

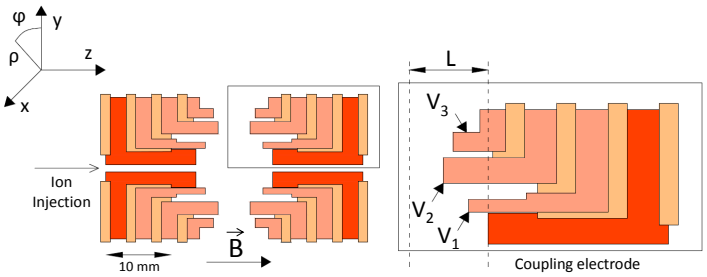

Figure 4: Technical drawing of a longitudinal cut of the modified open-ring trap, which has revolution symmetry along the z-axis. For the final system, the scale is reduced by a factor of 10. The previously existing electrodes are shown in dark orange, the one added in this work is shown in red, and the insulators to fix the structure are shown in light orange.

The procedure of calculating the equipotential lines and performing the fit was repeated for several values of L. The final value was obtained by fitting a linear function to the data (C_4 versus L) and by solving for the zero of the fit function. After this, the size of the trap in Fig. 4 was reduced by a factor of 10. This is a good compromise to maintain the frequency shifts due to image charges as small as possible. Following the notation given in Ref. [22], where the author assumed a spherical trap, this frequency shift is given by:

$$\delta = \frac{3}{2}\frac{qc}{Ba^3}, \tag{23}$$

where a is the radius of the trap. Comparing the size of the trap developed in this work with the trap described in Ref. [8], it yields a shift δ a factor of 8 larger, which can be only counteracted by using the lowest electronic-charge states (1^{+}-2^{+}) of the heavy or superheavy ion. In addition, the ions can be easily shuttled into and from the system to another trap, making this method universal.

The final system comprises two identical traps, one for $^{187}Re^{+}$ (probed ion) and the other for $^{40}Ca^{+}$ (sensor ion). In order to study the suitability of the trap geometry, we will start with the calculation of the potential ΔU due to the charge induced and the transfer constant b defined in Eqs. (16) and (19), respectively. Table 1 gives the values of ΔU and b for the geometries shown in Figs. 3 and 4. For the calculations C_T = 10 pF and B = 7 T.

The planar trap was conceived for electrons and the work was focused on reducing the axial-frequency shift. These traps do not meet the requirements for heavy ions in terms of a low detection frequency, and simultaneous adjustment of frequency and frequency shifts, considering ion species with very different masses like $^{187}Re^{+}$ and $^{40}Ca^{+}$. Furthermore, the traps for these two ion species cannot be identical and the configuration does not allow for injection of ions created externally.

The cylindrical trap might be more suitable than the open-ring trap, since the charge induced by the probed ion in the interconnected image-current sensing electrodes is larger by a factor of $\sim$ 2 (if ρ_0 = 1 mm). Both geometries permit the injection of ions created outside the trap as it happens in the project TRAPSENSOR. However, the open geometry of the ring trap allows accessing radially the $^{40}Ca^{+}$ ion with the lasers and collecting fluorescence photons, opposite to the cylindrical trap where one would need to create holes, modifying the radial symmetry of the trap potential.

5. Micro-trap implementation

The double Penning-trap system has been microfabricated using laser-induced etching processes [32] and standard metallization techniques. The ion trap is structured on fused silica with a depth of 40-60 μm by laser induced wet etching. The trap electrodes are grown by sputtering of Au on top of the microstructured fused-silica substrates.

The electrode configuration shown in Fig. 4, and scaled down by a factor of 10, was modified again for the fabrication. The final micro Penning-trap system is an arrangement of several

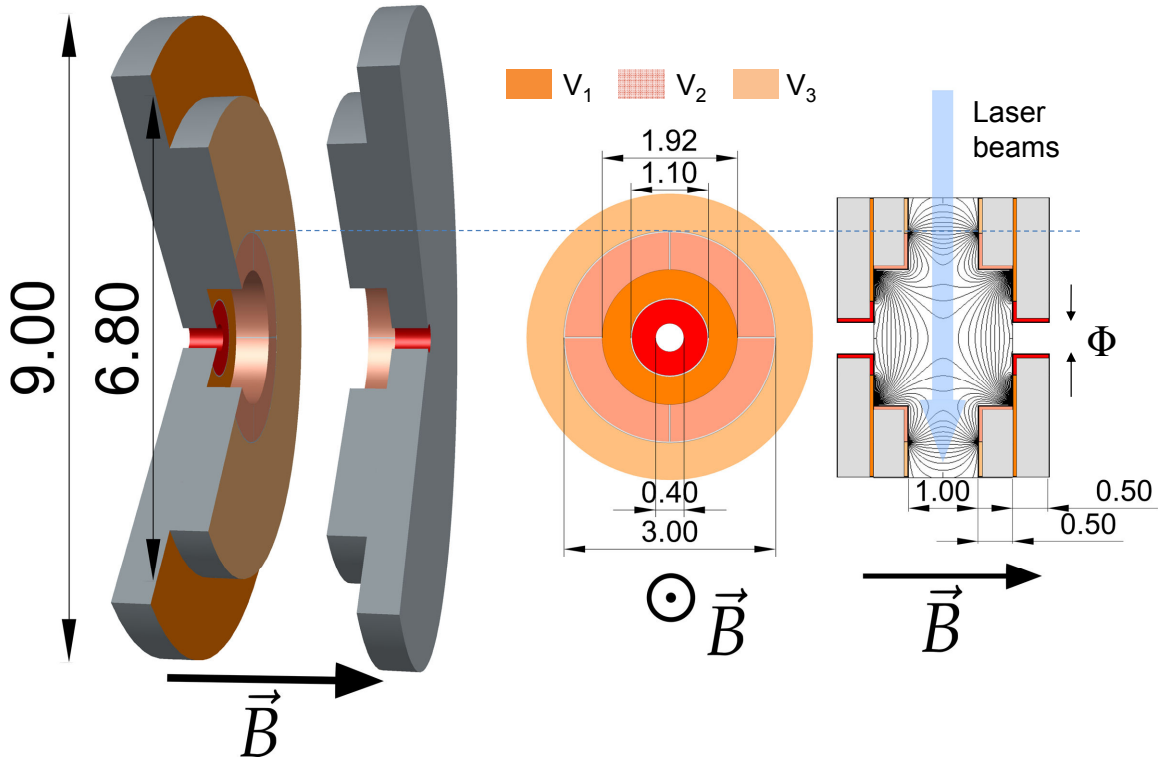

Figure 5: Right: cut from a 3D-CAD drawing of a Penning trap made of disks, indicating the dimensions in millimeters. Center: front view of two contiguous fused-silica wafers. The electrodes used for ion-ion coupling are shown in red and dark orange. Two of the electrodes are four-fold segmented to apply external radiofrequency fields allowing for axialization (sensor ion), excitation of the ion's eigenmotions and side-band drives in both traps. Right: longitudinal view showing the equipotential lines of the quadrupole field. $\Phi = 400\ \mu$m. The horizontal dotted line serves to indicate the fraction of the fused-silica wafers shown in the two dimensional views.

disks made of fused-silica wafers with a thickness of 500 μm. A cut of a 3D view of one trap, made of four wafers, each of them containing two electrodes, is shown on the left side in Fig. 5. The center shows a front view of two contiguous wafers, where the electrodes for ion-ion coupling are marked in red and dark orange, and the right side shows a longitudinal cut with the equipotential lines generated by the quadrupole electric field. The injection of the ion/s into the trap is very important for the final design. Micro-traps are used often in experiments where ions are created inside the trap, either by electron bombardment or by photoionization [26]. The final goal in the project TRAPSENSOR is to use ions created outside the trap by laser desorption [33], which are injected into a so-called preparation Penning trap, where cooling and mass separation is performed [34], to be finally transferred into the double micro Penning-trap system where they enter through a hole with a diameter Φ (see Fig. 5).

The optimization procedure, in order to adjust the C_2 and C_4 terms, is an iterative process fixing V_3 and the voltage on the coupling electrode to 0 V, and following the two steps given below:

- Fixing $R_v = -V_2/V_1$, a value of V_2 is obtained which makes $\nu_z = 100$ kHz.

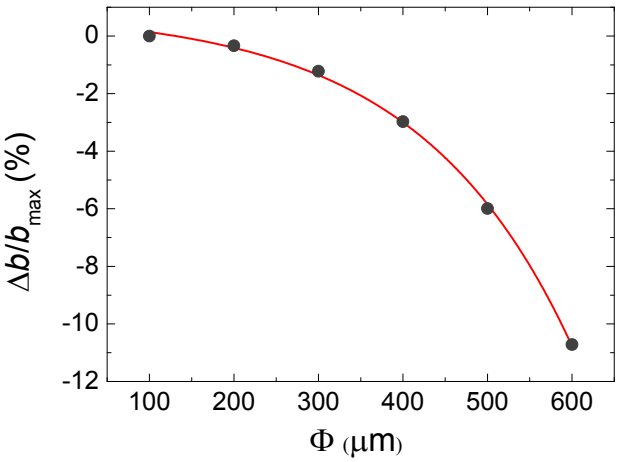

Figure 6: Deviation (decrease) of the parameter b as a function of the aperture Φ of the trap for injection of the ions.

- Maintaining V_2 constant, a value of R_v that makes $C_4 = 0$ is deduced.

At the end, a fine adjustment for the final frequency as a function of V_2 with C_2 and C_4 almost constant is performed. This has been done for several apertures. A larger aperture would favor the injection of the ion but will reduce the

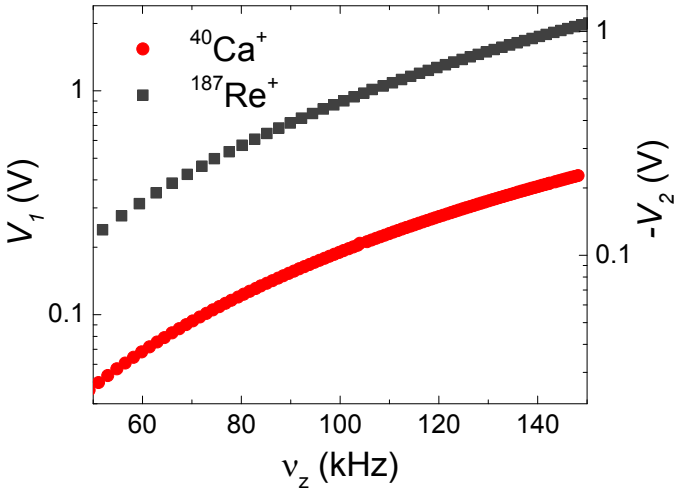

Figure 7: Voltages V_1 and V_2 (Fig. 5) as a function of the axial oscillation frequency for $^{40}Ca^+$ and $^{187}Re^+$. R_v is constant, and $\Delta\nu_z$ (Eq. 22) is kept below 0.4 Hz. The final values of V_1 and V_2 to operate the traps will be biased to match the kinetic energies of the injected ions.

coupling strength quantified here through the parameter b, (see Eq. (20)). Figure 6 shows the relative deviation of the parameter b as a function of Φ. The final value of $\Phi = 400\ \mu$m was adopted, which is a good compromise. C_4 is in the order of 10^{-8} V/(100μm)^2, $R_v(^{40}Ca^+) = 1.8419$ and $R_v(^{187}Re^+) = 1.8633$. $\Delta\nu_z$ is 0.1 mHz for $^{40}Ca^+$ at 1 mK, and 0.07 Hz for $^{187}Re^+$ at 5 K. b_1 (coupling electrode, depicted in red in Fig. 5) is 3.24×10^{-7} m/s, which is a factor of ~ 3 larger than b_2 (V_1 in Fig. 5, depicted in dark orange). The oscillation frequency of the ions in the trap can be easily tuned maintaining R_v constant, and varying $V_1(V_2)$ as shown in Fig. 7.

Simulations were carried out using SIMION to study the trapping efficiency. Figure 8 shows the potential shape along the z-axis to trap the ions in the double micro Penning-trap system. The ions are first trapped, and cooled in a preparation Penning trap (PPT) [34]. Thereafter they are released to the double micro Penning-trap system. A 2D drawing of this section is shown on top. The PPT, diaphragm and first lens in the time-of-flight (TOF) section are colored in grey scale. $z = 0$ is taken as the center of the distance between the two homogeneous regions of the magnetic field. The dotted-red line is the potential shape for ion injection in the first (A) and second trap (B). The solid-blue line is the potential shape to trap ions in the micro-traps system. Figure 9 shows the expected trapping efficiency for $^{40}Ca^+$ ions as a function of the waiting time after the ions are extracted from the PPT. 1000 ions within an energy distribution around 300 K, were fired in these simulations to obtain each data point. The ion distributions were built from the results of the measurements carried out with the PPT. All ions entering the trap system are trapped. However, only about 20% of the ions delivered by the PPT after applying the buffer-gas cooling technique [35], pass through the nozzle-type diaphragm.

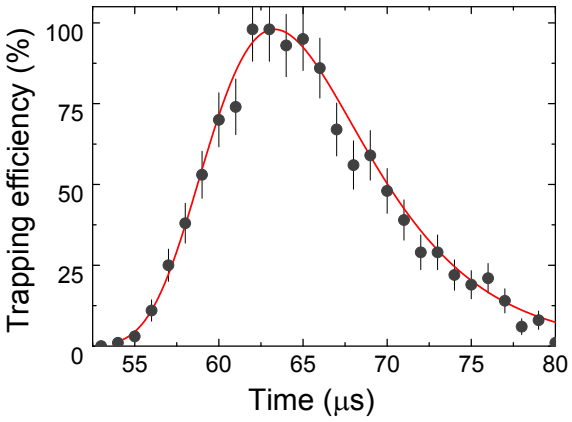

Figure 9: Results from the simulations performed with SIMION to trap $^{40}Ca^+$ ions in the second micro Penning-trap of Fig. 8. More details are given in the text.

5.1. Electronics for ion-ion coupling

The stability in frequency required during the energy exchange process is related to the time (t_{ex}) needed to exchange the energy between the probed and the sensor ions given by [19]

$$t_{ex} = 2\pi^2 \nu_z C_T \left(\frac{D}{\alpha q_s}\right)\left(\frac{D}{\alpha q_{pr}}\right)\sqrt{m_s m_{pr}}, \quad (24)$$

where $D \approx 2z_0$, q_{pr} and q_s are the electronic charge states of the probed and sensor ions, respectively, and m_{pr} and m_s, their masses. The geometrical factor α [19] is 0.62645 for the trap developed in this work. Under these conditions, the frequency should be stable within the range from 3.5 to 10 mHz in order to achieve an efficient ion-ion coupling for singly-charged ions in the mass range from 40 to 270. Using Eq. (9), the relative voltage variation has to be between $1 \times 10^{-7}(^{270}Db^+)$ and $2.6 \times 10^{-7}(^{40}Ca^+)$. The Allan curve [36] obtained from the measurements, when setting the voltage to 0.8 V, has yielded a relative voltage stability around 1.2×10^{-7}, even when the voltage source was connected to the digital multimeter through a low-noise switch. For all the calculations $C_T = 1$ pF, which is a factor of 3 larger compared to the value quoted in Ref. [19]. In order to have small capacitances, the electronic circuits are located at the shortest possible distance (Millimeters) to the traps, completely surrounding the electrode disks.

The circuit diagram of the electronics for each of the traps of the double micro Penning-trap system is shown in the upper part of Fig. 10. These electronics consist of low pass filters in order to ensure a noise free and electrically stable environment for the ions, and provide the possibility to monitor their axial motion using image charge detection by tailored cryogenic low noise GaAs FETs (transistor S in the figure). As one can see in the inset of the lower part, electronics and trap structure are merged together into the same geometrical plane, forming a novel functional entity of trap and electronics. This allows minimizing all

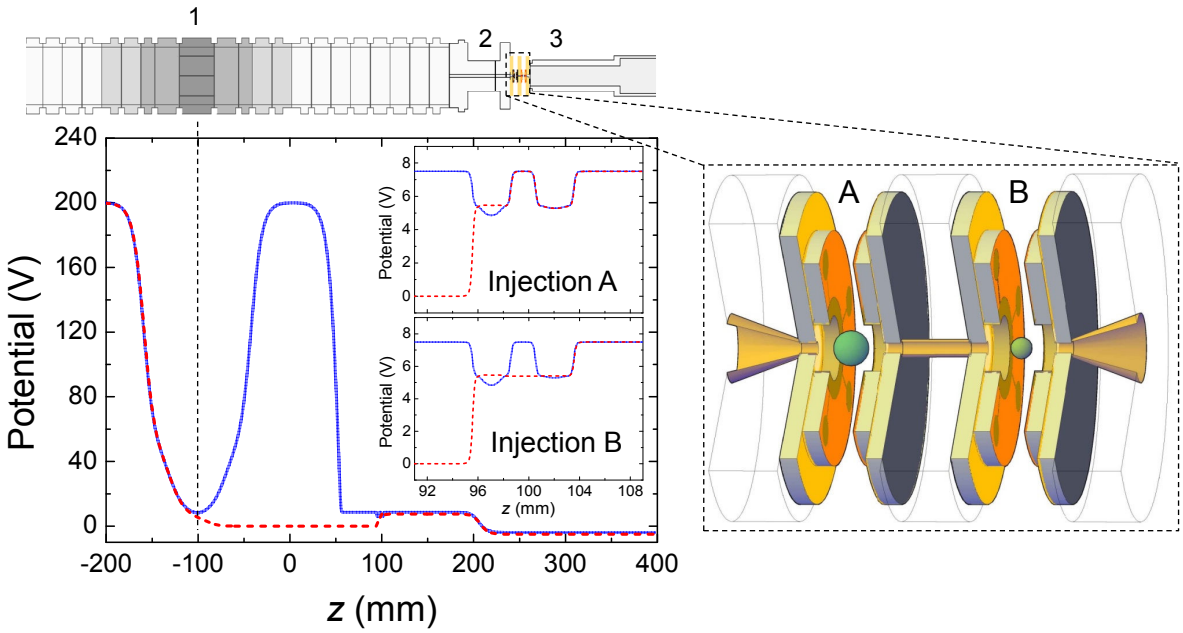

Figure 8: Left: Shape of the potential along the z-axis from the center of the preparation Penning trap (1) [34] to capture and to eject afterwards the ions into the double micro Penning-trap system. (2) indicates a pumping barrier and (3) the beginning of the time-of-flight section behind the traps. Right: Zoom of a 3D CAD drawing of the double micro Penning-trap system. The support disks for the trap assembly are not colored and the electronics is not shown.

parasitic stray capacitances, thus optimizing the ion-ion coupling efficiency and achieving higher ion detection sensitivity. The electrodes on the left side are pulsed together with the nozzle to capture the ions. V_1, V_2 and V_3 were defined in Fig. 5. There is no specific electrical switch for ion-ion coupling, even though the design is already prepared for utilizing a FET switch for this purpose, but the ions will be coupled or decoupled by adjusting the trapping potential which defines the axial oscillation frequency of one of them. The induced image charge is picked up from the coupling (R) and E1 electrodes, which are coupled together for AC but decoupled for DC via C_C. The capacitor C_F provides an image charge signal to be connected to the adjacent trap for ion-ion coupling. The lower part shows a picture of the system assembled with the electronics printed circuit boards made of Rogers 4350B material with a thickness of 0.76 mm and a copper layer of 35 μm [37]. These PCBs can be seen more clearly in the inset.

6. Conclusions and outlook

The work presented in this paper has resulted in an optimal configuration for the double micro Penning-trap system to be built within the project TRAPSENSOR in order to perform high-precision mass measurements using a laser-cooled ion as a detector. This technique should provide unprecedented sensitivity, since very small oscillation amplitudes of the probed ion will be detected. In order to choose the electrode configuration, an exhaustive study using analytical and numerical methods has been carried out to calculate the electrostatic potential generated by three different geometries: 1) a planar trap conceived for experiments with electrons [27, 28], 2) the conventional cylindrical trap [29], which is used for example for preparation of the ions in the project TRAPSENSOR, and 3) the open-ring trap, which might be considered as a modified geometry from the original hyperbolic trap. This trap has been successfully tested showing laser cooling on a single $^{40}Ca^{+}$ ion [26].

After deciding on the geometry to be used, this was adapted to a microfabrication process. The electronics was inserted in a printed circuit board made of Rogers material (4350B), and tested with a cold-head system down to 4 K before it was assembled to the system. The on-going work is presently focussed on the construction of the optical and cryogenic systems to operate the double micro Penning-trap system in the Penning-traps beamline of the TRAPSENSOR facility at the University of Granada.

Acknowledgement

We acknowledge support from the European Research Council (ERC StG contract no 278648-TRAPSENSOR) and from the Spanish Ministry of Economy and Competitiveness through the projects FPA2012-32076, FPA2015-67694-P and UNGR10-1E-501. We also acknowledge support from ERC StG "QLEDS" and PTB clean room facility staff. We warmly thank José Verdú and Pierre Delahaye for providing the programs they developed for their traps to be used for the calculations presented here. Part of the work of M.J.G. was supported by a fellowship on initiation to research provided by the so-called "Plan Propio" funded by the Vice-Rectorate of

Scientific Policy and Research at the University of Granada.

References

[1] M. P. Bradley, J. V. Porto, S. Rainville, J. K. Thompson, D. E. Pritchard, Penning Trap Measurements of the Masses of ^{133}Cs, ^{87,85}Rb, and ^{23}Na with Uncertainties ≤ 0.2 ppb, Physical Review Letters 83 (1999) 4510–4513. doi:10.1103/PhysRevLett.83.4510.

[2] S. Rainville, J. K. Thompson, D. G. Myers, J. M. Brown, M. S. Dewey, E. G. Kessler Jr., R. D. Deslattes, H. G. Börner, M. Jentschel, P. Mutti, D. E. Pritchard, World Year of Physics: A direct test of E=mc^2, Nature 438 (2005) 1096–1097. doi:10.1038/4381096a.

[3] M. Redshaw, J. McDaniel, E. G. Myers, Dipole Moment of PH^+ and the Atomic Masses of ^{28}Si, ^{31}P by Comparing Cyclotron Frequencies of Two Ions Simultaneously Trapped in a Penning Trap, Physical Review Letters 100 (2008) 093002. doi:10.1103/PhysRevLett.100.093002.

[4] S. Sturm, F. Köhler, J. Zatorski, A. Wagner, Z. Harman, G. Werth, W. Quint, C. H. Keitel, K. Blaum, High-precision measurement of the atomic mass of the electron, Nature 506 (2014) 467–470. doi:10.1038/nature13026.

[5] D. J. Wineland, H. G. Dehmelt, Principles of the stored ion calorimeter, Journal of Applied Physics 46 (1975) 919. doi:10.1063/1.321602.

[6] E. A. Cornell, R. M. Weisskoff, K. R. Boyce, R. W. Flanagan Jr., G. P. Lafyatis, D. E. Pritchard, Single-ion cyclotron resonance measurement of $M(CO^+)/M(N_2^+)$, Physical Review Letters 63 (1989) 1674–1677. doi:10.1103/PhysRevLett.63.1674.

[7] R. S. Van Dyck Jr., D. L. Farnham, P. B. Schwinberg, Precision mass measurements in the UW-PTMS and the electron's "atomic mass", Physica Scripta T59 (1995) 134-143. doi:10.1088/0031-8949/1995/T59/017.

[8] R. S. Van Dyck Jr., D. B. Pinegar, S. V. Liew, S. L. Zafonte, The UW-PTMS: Systematic studies, measurement progress, and future improvements, International Journal of Mass Spectrometry 251 (2006) 231–242. doi:10.1016/j.ijms.2006.01.038.

[9] S. Streubel, T. Eronen, M. Höcker, J. Ketter, M. Schuh, R. S. Van Dyck Jr., K. Blaum, Toward a more accurate Q value measurement of tritium: status of THe-Trap, Applied Physics B: Lasers and Optics 114 (2014) 137–145. doi:10.1007/s00340-013-5669-x.

[10] J. Angrik, *et al.*, Technical Report, Karlsruher Institut für Technologie (KIT) (unpublished)

[11] Mare proposal, downloadable from: http://crio.mib.infn.it/wig/silicini/publications.html.

[12] P. C. O. Ranitzsch, J. P. Porst, S. Kempf, C. Pies, S. Schäfer, D. Hengstler, A. Fleischmann, C. Enss, L. Gastaldo, Development of Metallic Magnetic Calorimeters for High Precision Measurements of Calorimetric ^{187}Re and ^{163}Ho Spectra, Journal of Low Temperature 167 (2012) 1004–1014. doi:10.1007/s10909-012-0556-0.

[13] B. Alpert, M. Balata, D. Bennett, M. Biasotti, C. Boragno, C. Brofferio, V. Ceriale, D. Corsini, P. K. Day, M. D. Gerone, M. F. R. Dressler, E. Ferri, J. Fowler, F. Gatti, A. Giachero, J. Hays-Wehle, S. Heinitz, G. Hilton, U. Köster, M. Lusignoli, M. Maino, J. Mates, S. Nisi, R. Nizzolo, A. Nucciotti, G. Pessina, G. Pizzigoni, A. Puiu, S. Ragazzi, C. Reintsema, M. R. Gomes, D. Schmidt, D. Schumann, M. Sisti, D. Swetz, F. Terranova, J. Ullom, The electron capture decay of ^{163}Ho to measure the electron neutrino mass with sub-eV sensitivity, European Physical Journal C 75 (2015) 112. doi:10.1140/epjc/s10052-015-3329-5.

[14] https://p25ext.lanl.gov/~kunde/NuMECS/.

[15] M. Block, D. Ackermann, K. Blaum, C. Droese, M. Dworschak, S. Eliseev, T. Fleckenstein, E. Haettner, F. Herfurth, F. P. Hessberger, S. Hofmann, J. Ketelaer, J. Ketter, H.-J. Kluge, G. Marx, M. Mazzocco, Y. N. Novikov, W. R. Plass, A. Popeko, S. Rahaman, D. Rodríguez, C. Scheidenberger, L. Schweikhard, P. G. Thirolf, G. K. Vorobyev, C. Weber, Direct mass measurements above uranium bridge the gap to the island of stability, Nature 463 (2010) 785–788. doi:10.1038/nature08774.

[16] E. Minaya Ramirez, D. Ackermann, K. Blaum, M. Block, C. Droese, C. E. Düllmann, M. Dworschak, M. Eibach, S. Eliseev, E. Haettner, F. Herfurth, F. Hessberger, S. Hofmann, J. Ketelaer, G. Marx, M. Mazzocco, D. Nesterenko, Y. N. Novikov, W. Plass, D. Rodríguez, C. Scheidenberger, L. Schweikhard, P. G. Thirolf, C. Weber, Direct Mapping of Nuclear Shell Effects in the Heaviest Elements, Science 337 (2012) 1207–1210. doi:10.1126/science.1225636.

[17] E. Minaya Ramirez, D. Ackermann, K. Blaum, M. Block, C. Droese, C. E. Düllmann, M. Eibach, S. Eliseev, E. Haettner, F. Herfurth, F. Hessberger, S. Hofmann, G. Marx, D. Nesterenko, Y. N. Novikov, W. Plass, D. Rodríguez, C. Scheidenberger, L. Schweikhard, P. G. Thirolf, C. Weber, Recent developments for high-precision mass measurements of the heaviest elements at SHIPTRAP, Nuclear Instruments and Methods in Physics Research Section B: Beam Interactions with Materials and Atoms 317 (2013) 501–505. doi:10.1016/j.nimb.2013.07.055.

[18] D. Rodríguez, A quantum sensor for high-performance mass spectrometry, Applied Physics B: Lasers and Optics 107 (2012) 1031–1042. doi:10.1007/s00340-011-4824-5.

[19] D. J. Heinzen, D. J. Wineland, Quantum-limited cooling and detection of radio-frequency oscillations by laser-cooled ions, Physical Review A 42(5) (1990) 2977–2994. doi:10.1103/PhysRevA.42.2977.

[20] D. Leibfried, R. Blatt, C. Monroe, D. Wineland, Quantum dynamics of single trapped ions, Review of Modern Physics 75 (2003) 281–324. doi:10.1103/RevModPhys.75.281.

[21] R. S. Van Dyck, Jr., F. L. Moore, D. L. Farnham, P. B. Schwinberg, Number dependency in the compensated Penning trap, Physical Review A, 40 (1989) 6308-631. doi:10.1103/PhysRevA.40.6308.

[22] J. V. Porto, Series solution for the image charge fields in arbitrary cylindrically symmetric Penning traps, Physical Review A, 64 (2001) 023403/1-7. doi:10.1103/PhysRevA.64.023403.

[23] H. Häffner, T. Beier, S. Djekic, N Hermanspahn, H.-J. Kluge, W. Quint, S. Stahl, J. Verdú, T. Valenzuela, G. Werth, European Physical Journal D, 22 (2003) 163-182. doi:10.1140/epjd/e2003-00012-2.

[24] J. M. Cornejo, D. Rodríguez, A Quantum Sensor for Neutrino Mass Measurements, Advances in High Energy Physics 849497 (2012) 1. doi:10.1155/2012/849497.

[25] L. S. Brown, G. Gabrielse, Geonium theory: Physics of a single electron or ion in a Penning trap, Review of Modern Physics 58 (1986) 233–311. doi:10.1103/RevModPhys.58.233.

[26] J. M. Cornejo, M. Colombano, J. Doménech, M. Block, P. Delahaye, D. Rodríguez, Extending the applicability of an open-ring trap to perform experiments with a single laser-cooled ion, Review of Scientific Instruments 86 (2015) 103104. doi:10.1063/1.4932310.

[27] J. Goldman, G. Gabrielse, Optimized planar Penning traps for quantum-information studies, Physical Review A 81 (2010) 052335. doi:10.1103/PhysRevA.81.052335.

[28] S. Stahl, F. Galve, J. Alonso, S. Djekic, W. Quint, T. Valenzuela, J. Verdú, M. Vogel, G. Werth, A planar Penning trap, European Physical Journal D 32 (2005) 139–146. doi:10.1140/epjd/e2004-00179-x.

[29] G. Gabrielse, L. Haarsma, S. L. Rolston, Open-endcap Penning traps for high precision experiments, International Journal of Mass Spectrometry and Ion Processes 88 (1989) 319–322. doi:10.1016/0168-1176(89)85027-X.

[30] B. G. Olmedo, Fundamentos de Electromagnetismo, Iniciación al Cálculo Numérico en Electromagnetismo, Universidad de Granada.

[31] J. Verdú, Theory of the coplanar-waveguide Penning trap, New Journal of Physics 13 (2011) 113029. doi:10.1088/1367-2630/13/11/113029.

[32] A. Marcinkevicius, S. Juodkazis, M. Watanabe, M. Miwa, S. Matsuo, H. Misawa, J. Nishii, Femtosecond laser-assisted three-dimensional microfabrication in silica, Optics Letters 26 (2001) 277–279. doi:10.1364/OL.26.000277.

[33] J. M. Cornejo, A. Lorenzo, D. Renisch, M. Block, C. E. Düllmann, D. Rodríguez, Status of the project TRAPSENSOR: Performance of the laser-desorption ion source, Nuclear Instruments and Methods in Physics Research Section B: Beam Interactions with Materials and Atoms 317 (2013) 522–527. doi:10.1016/j.nimb.2013.05.060.

[34] J. M. Cornejo, D. Rodríguez, A preparation penning trap for the TRAPSENSOR project with prospects for MATS at FAIR, Nuclear Instruments and Methods in Physics Research Section B: Beam Interactions with Materials and Atoms 376 (2016) 288–291. doi:10.1016/j.nimb.2015.11.033.

[35] G. Savard, S. Becker, G. Bollen, H. J. Kluge, R. B. Moore, T. Otto, L. Schweikhard, H. Stolzenberg, U. Wiess, A new cooling technique for heavy ions in a Penning trap, Physics Letters A 158 (1991) 247–252. doi:10.1016/0375-9601(91)91008-2.

[36] C.A. Greenhall, Frequency Stability Review, TDA Progress Report 42

(1987).
[37] https://www.rogerscorp.com/acs/products/55/RO4350B-Laminates.aspx

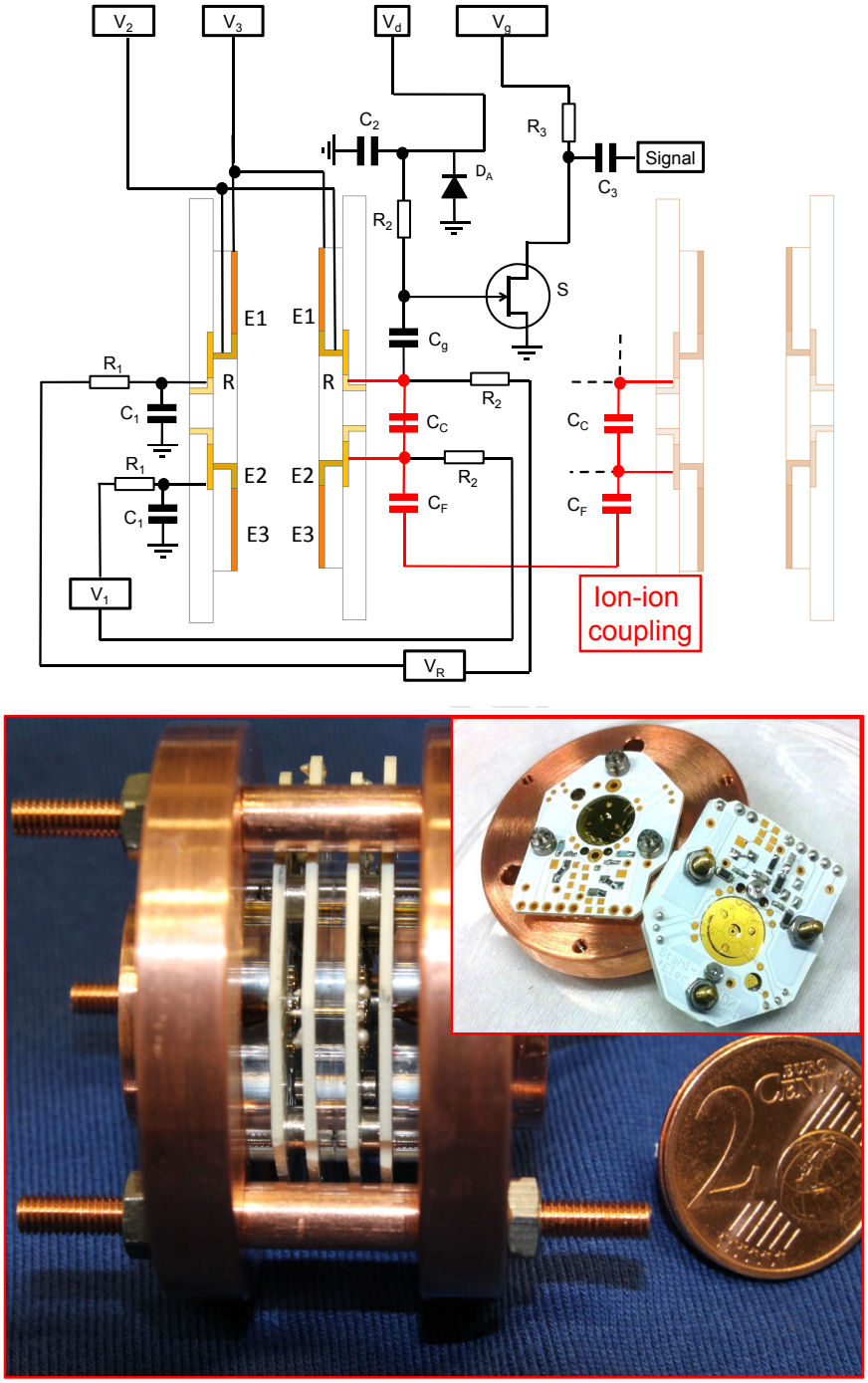

Figure 10: Top: Diagram of the electronic circuit to operate one of the traps in the double micro Penning-trap system. The path for charge flow between the traps to perform ion-ion coupling is shown in red. The rest of the circuitry for the second trap is identical. The voltages are defined as in Fig. 5, except V_R, which represents a voltage applied to the coupling electrode. Bottom: Picture of the double micro Penning-trap system. The inset (at different scale) shows the electrodes on the left and right of one trap, assembled with the electronics printed circuit boards. Further details are given in the text.